SARS-CoV-2 uses clathrin-mediated endocytosis to gain access into cells

Running title:COVID-19 and endocytosis

Armin Bayati*, Rahul Kumar*, Vincent Francis, and Peter S. McPherson

Department of Neurology and Neurosurgery, Montreal Neurological Institute, McGill University, Montreal, QC, Canada

* These two authors contributed equally to this study

Address correspondence to:
Dr. Peter S. McPherson
Department of Neurology and Neurosurgery
Montreal Neurological Institute
McGill University
3801 University Street
Montreal, QC H3A 2B4
Canada
phone: (514) 398-7355
Email: peter.mcpherson@mcgill.ca

Abstract

With more than 13 million cases and 570,000 deaths, and with the resulting social upheaval, the COVID-19 pandemic presents one of the greatest challenges ever to the scientific community. It is thus vital to fully understand the biology of SARS-CoV-2, the causative agent of COVID-19. SARS-CoV-2 uses the spike glycoprotein to interact with the cell surface and to drive fusion of the viral membrane with cellular membranes, thus allowing transfer of viral RNA to the cytosol. Here we use purified spike glycoprotein protein and lentivirus pseudotyped with spike glycoprotein to determine that SARS-CoV-2 undergoes rapid endocytosis following binding to the plasma membrane. Using chemical inhibitors and loss of function approaches, we demonstrate that this cellular entry is through clathrin-mediated endocytosis. Thus, it appears that SARS-CoV-2 first engages the plasma membrane, then rapidly enters the lumen of the endosomal system, strongly suggesting that fusion of the viral membrane occurs with the lumenal membrane of endosomes. This discovery has important implications for the development of chemical probes to reduce or block infection.

The internal membrane system represents a major evolutionary advance associated with the emergence of the eukaryotic cell. Its dynamics are integral to basic cellular function and underlie much of the novel capability of the cell, including the almost infinite range of physiological responsiveness required for the complexity of eukaryotic organisms. Unfortunately, viruses subvert this complexity to gain access into cells and to propagate in a manner that allows them to limit immune surveillance. Antiviral strategies targeting the earliest steps of infection, such as cellular entry are appealing, as interference through a common, early step can provide robust efficacy. Thus, understanding the mechanisms of viral cellular entry is crucial.

As of July 13, 2020 there are over 13 million confirmed cases of COVID-19 worldwide with ~570,000 deaths (coronavirus.jhu.edu). However, studies of antibody seroprevalence in broad communities have indicated that approximately 3-20% of total populations have been exposed to severe acute respiratory syndrome coronavirus-2 (SARS-CoV-2), the COVID-19 causing virus (Bendavid et al., 2020; Goodman and Rothfeld, 2020). It thus appears that infection rates are dramatically higher than viral tests indicate, but far below a level that would begin to allow herd immunity. Despite the prevalence and worldwide impact of COVID-19 on human health and the global economy, many aspects of fundamental virus biology remain unknown. Notably, it is not understood how SARS-CoV-2 enters cells.

Since the beginning of the 21st century, 3 coronaviruses have crossed the species barrier to cause deadly pneumonias in humans; Middle-East respiratory syndrome coronavirus (MERS-CoV) (Zaki et al., 2012), SARS-CoV (Drosten et al., 2003; Ksiazek et al., 2003), and SARS-CoV-2 (Huang et al., 2020; Zhu et al., 2020). All originated in bats but zoonotic transmission involved intermediate hosts; dromedary camels (MERS-CoV), civets (SARS-CoV), and unknown (SARS-CoV-2). The presence of numerous coronaviruses in bats suggests that zoonotic transmission to humans will continue (Tortorici and Veesler, 2019), and new pandemic potential viruses continue to emerge (Sun et al., 2020).

Coronavirus entry into hosts cells is mediated by the transmembrane spike (S) glycoprotein, which forms homotrimers (Tortorici and Veesler, 2019). The S protein from SARS-CoV-2 is composed of S1 and S2 subdomains (Wrapp et al., 2020). The S1 subdomain encodes the receptor binding domain and is responsible for binding to host cells, whereas the S2 subdomain contains the transmembrane domain and is responsible for fusion of the viral membrane with

cellular membranes. The receptor for the S glycoprotein is angiotensin converting enzyme 2 (ACE2) (Hoffmann et al., 2020; Letko et al., 2020; Zhou et al., 2020; Walls et al. 2020). ACE2 is a transmembrane metallopeptidase localized primarily on the plasma membrane with abundant expression in lung alveolar epithelial cells (Hamming et al., 2004). The receptor binding domain of the S protein binds ACE2 with low nM affinity, allowing the virus to stably associate with the plasma membrane (Walls et al., 2020). Cleavage of the S glycoprotein between the S1 and S2 domains, mediated by the type II transmembrane serine protease TMPRSS2 (Hoffmann et al., 2020), and perhaps by furin, activates the S2 subdomain. The S2 subdomain then mediates the fusion of the viral membrane and the cellular membrane in a process that is a molecular mimic of SNARE-mediated fusion of cellular membranes (Walls et al., 2020; Hamming et al., 2020; Weber et al., 1998). This creates a pore allowing the RNA and RNA-associated proteins in the lumen of the virus to gain access to the cellular cytosol, triggering infection.

Surprisingly, for SARS-CoV-2, it remains unknown where the fusion of the viral and cellular membranes occurs. One possibility is that fusion occurs at the cell plasma membrane and this has been proposed as the major cellular entry pathway (Tang et al., 2020). In such a scenario, the virus coat proteins do not directly enter the cell, but the RNA that enters the cytosol through the fusion pore drives infection. Alternatively, the ACE2/SARS-CoV-2 complex may undergo endocytosis with the entire virus, including the capsid proteins, being rapidly brought into the cell. In this scenario, the viral membrane would fuse with the luminal face of the endosomal membrane, allowing for RNA transfer to the cytosol. This mechanism has been proposed as an alternative to RNA transfer at the cell surface (Glebov, 2020; Yang and Shen, 2020). If the virus enters by endocytosis it is important to determine which of the many endocytic entry pathways it uses. SARS-CoV S glycoprotein binds ACE2 to initiate infection so lessons from this virus are highly relevant to SARS-CoV-2. For SARS-CoV, it has been suggested that endocytosis may be the first step in infectivity and two endocytic mechanisms have been proposed. The first indicates that SARS-CoV uses clathrin-mediated endocytosis (CME) (Inoue et al., 2020) to gain access into cells. A second study states the exact opposite, that SARS-CoV S protein binds to ACE2 allowing for viral endocytosis, but in a clathrin-independent process (Wang et al., 2020). Here we demonstrate rapid endocytosis of SARS-CoV-2 using purified S protein and lentivirus pseudotyped with the S protein. We discover that this process is sensitive to inhibitors of CME and genetic manipulations that block CME. Our data provides new insight into cellular entry of SARS-CoV-2 and indicates a mechanism that could be targeted for therapeutic benefit.

Results

SARS-CoV-2 S glycoprotein binds to the surface of HEK-293T cells in an ACE2-dpendent manner

We first sought to generate a model system to examine for potential SARS-CoV-2 endocytosis. The S glycoprotein is critical for binding ACE2, for driving the association of SARS-CoV-2 with the plasma membrane, and for allowing virus infectivity (Tortorici and Veesler, 2019; Wrapp et al., 2020; Hoffmann et al., 2020; Letko et al., 2020; Zhou et al., 2020; Walls et al., 2020; Hamming et al., 2020; Weber et al., 1998). We obtained HEK-293T cells expressing ACE2 (HEK-293T-ACE2) from Dr. Jesse Bloom (University of Washington) (Crawford et al., 2020). Wild-type HEK-293T cells or HEK-293T-ACE2 were incubated for 30 min on ice with purified S protein. Following a PBS wash, S protein is seen to bind to the plasma membrane of cells expressing ACE2 but not to the control HEK-293T cells (Fig. 1A), which have very low endogenous levels of the ACE2 receptor (Fig. 6A). In contrast, transferrin (Trf), which binds to the Trf receptor, interacts with the surface of the cells independent of their ACE2 status (Fig. 1A). Following a brief acid wash, both S protein and Trf are stripped from the surface of cells (Fig. 1B). Thus, HEK-293T cells lacking or expressing ACE2 appear are a functional model system for examining potential SARS-CoV-2 endocytosis.

SARS-CoV-2 S protein is rapidly internalized into cells in an ACE2-dependent manner

We tested for endocytosis using two ligands, lentivirus in which the VSV-G glycoprotein was removed and substituted with the S glycoprotein form SARS-CoV-2 (Fig. 9) (Crawford et al., 2020) and purified S glycoprotein. While using purified S protein is a reductionist approach, from the point of view of the cell and ACE2, it is unlikely that receptor binding and initial membrane trafficking depends on whether or not there is a particle attached to the S protein. For example, epidermal growth factor and insulin undergo similar cell surface binding and CME as purified proteins or when attached to magnetic beads (Li et al., 2005). We thus added purified S protein to HEK-293T cells, wild-type or expressing ACE2. Following 30 min on ice, the cells where transferred to 37°C for an additional 30 min. Following this treatment, cells were washed briefly with acid to strip off any surface bound S protein. Remarkably, S protein was internalized into the cells (as revealed by its resistance to acid wash) in an ACE2-dependent manner (Fig. 2). In contrast, Trf was internalized independent of ACE2 (Fig. 2). We next examined the time course of internalization. S protein is internalized into cells rapidly and is detected in cells within 5 min

(Fig. 3), a hallmark of endocytosis. The amount of S protein in cells continues to increase for up to 45 min (Fig. 3). Thus, SARS-CoV-2 spike protein appears to entry cells via endocytosis.

SARS-CoV-2 S protein is internalized by CME

There are multiple endocytic mechanisms used by viruses and there are conflicting reports about SARS-CoV endocytosis (Inoue et al., 2020; Wang et al., 2020). We thus examined the internalization of SARS-CoV-2 in the presence of two drugs that are known to block CME, dynasore and Pitstop 2 (Marcia et al., 2006; von Kliest et al., 2011). Dynasore blocks the GTPase dynamin that drives the fission of clathrin-coated pits (CCPs) from the plasma membrane and Pitstop 2 prevents clathrin heavy chain (CHC) from interacting with adaptor proteins required for CCP formation (Marcia et al., 2006; von Kliest et al., 2011). Interestingly, both drugs dramatically reduce the endocytosis of SARS-CoV-2 S protein, strongly suggesting it is internalized by CME (Fig. 4A/B). Both dynasore and Pitstop 2 have been criticized for having off target effects (Park et al., 2013; Lemon and Traub, 2012). Therefore, we took a loss of function approach to inhibit CME by knockdown of CHC with a previously defined siRNA pool (Galvez et al., 2007; Kim et al., 2011). Transfection of HEK-293T-ACE2 cells with the CHC siRNA led to an ~ 50% decrease in CHC levels when compared to cells transfected with a control siRNA (Fig. 5A). Importantly, CHC knockdown led to a significant reduction of S protein endocytosis (Fig. 5B/C). Thus, the SARS-CoV-2 S protein undergoes rapid internalization via CME.

SARS-CoV-2 S protein undergoes rapid endocytosis in cell lines expressing endogenous levels of ACE2

We next sought to examine endocytosis of SARS-CoV-2 S protein in cells expressing endogenous levels of the cellular receptor ACE2. We first tested VERO cells, a monkey kidney epithelial cell that is robustly infected by SARS-CoV-2 (Hoffmann et al., 2020). VERO cells have high levels of ACE2 expression that exceeds even that of HEK-293 cells with overexpression of ACE2 (Fig 6A). SARS-CoV-2 spike protein added to VERO cells undergoes rapid endocytosis with the protein appearing in the cells as early as 5 min (Fig 6B), as determined using an antibody that specifically recognizes the spike protein (Fig S1). The amount of internalized protein increase slightly over the next 25 min with the protein appearing as distinct punctae in the cells (Fig. 6). We next tested for SARS-CoV-2 endocytosis in A549 cells that are widely used as a type II pulmonary epithelial cell model, and which are moderately infectible by the virus (Hoffman et al., 2020). A549 cells have ACE2 expression levels similar to the ACE2

expressing HEK-293 cell (Fig. 6A). These cells endocytose purified S protein with the protein barely detectable inside the cells at 5 min but easily seen in the cells after 30 min of internalization (Fig. 7). As for the VERO cells, endocytosed S protein appears as distinct punctae (Fig. 7). Thus, endocytosis of SARS-CoV-2 occurs in multiple cell types.

Following endocytosis SARS-CoV-2 S protein has a distinct trafficking itinerary from Trf

Trf bound to Trf-receptor is an established cargo of the recycling endosomal pathway. The Trf/Trf-receptor complex enters cells via CME and rapidly transports to early endosomes. From there the complex recycles directly back to the plasma membrane, a fast recycling route, or is transported to Rab11-positive recycling endosomes before returning to the cell surface, the slow recycling pathway) (Stoorvogel et al., 1991). When co-incubated with cells, both Trf and S proteins are rapidly internalized and accumulate in cells over 30 min (Fig. 8). However, there is little or no co-localization of the two cargo proteins once internalized (Fig. 8), indicating that they have different trafficking itineraries.

Lentivirus pseudotyped with SARS-CoV-2 S glycoprotein requires clathrin for infectability

Thus far the endocytosis assays have been performed with purified S protein. Thus, it is important to determine if viral infectivity also proceeds in a clathrin-dependent process. The most commonly used tool to examine the ability of SARS-CoV-2 to infect cells employs a variety of viruses pseudotyped with the SARS-CoV-2 S glycoprotein. Such pseudotyped viruses involve transfection of HEK-293T cells with a viral packaging construct, a viral transfer vector encoding luciferase or GFP, and a plasmid encoding the S protein, and are based on murine leukemia virus (Walls et al., 2020), VSV (Kang et al., 2020), or lentivirus (Crawford et al., 2020) among others. We have used a lentiviral system in which VSVG was replaced with the SARS-CoV-2 S glycoprotein (Crawford et al., 2020). We first incubate the virus with HEK-293 cells, wild-type or overexpressing ACE2, and infection was monitored by GFP expression. At 12 hours of incubation, HEK-293T cells expressing ACE2 were infected, whereas little to no infection was seen with wild-type HEK-293T cells (Fig. 9A). We next repeated the experiment using HEK-293T cells expressing ACE2, but which were transfected with a control siRNA or an siRNA driving knockdown of CHC (Fig. 5A). Importantly, CHC knockdown led to an ~ 60% decrease in viral infectivity (Fig. 9B). Taken together, or data indicate that SARS-CoV-2 uses its spike protein to engage ACE2, driving CME of the virus/receptor complex, and that this process is required for viral infectivity.

Discussion

Strategic entry mechanism used by viruses to infect mammalian host cells are unique and highly variable across different viral families (Pelkmans and Helenius, 2003). Among the various routes employed, the majority of viruses use endosomal pathways to efficiently deliver virion components into the cytoplasm for productive infection (Yamauchi and Helenius, 2013). While the most commonly used endosomal pathway is CME (utilized for example by Semliki forest virus and Adenovirus 2 and 5), other forms of endocytosis are employed (Pelkmans and Helenius, 2003; Yamauchi and Helenius, 2013; Marsh and Helenius, 2006). These include caveolae-mediated endocytosis (e.g. Simian virus 40), lipid-raft-mediated endocytic pathways (e.g. Avian sarcoma leukosis virus), and macropinocytosis (e.g. poxviruses) (Pelkmans and Helenius, 2003; Yamauchi and Helenius, 2013; Marsh and Helenius, 2006).

Endosomal entry mechanisms provide many advantages to the viruses by allowing them to efficiently spread while evading host immune surveillance. Most importantly, gaining access to the endocytic system helps viruses to prevent exposure of the viral capsid proteins to the host immune system at the level of plasma membrane. Additionally, strategic use of endosomal pathway also ensures entry into cells with active membrane transport system as opposed to cells with no such means (e.g. erythrocytes), which would prevent active propagation of the virus (Pelkmans and Helenius, 2003). Further, the acidic milieu of endosomes helps the incoming viruses to elicit penetration into the host cytosol (Pelkmans and Helenius, 2003; Marsh and Helenius, 2006).

The mostly closely related virus to SARS-CoV-2 is SARS-CoV. For SARS-CoV, endocytic entry has been suggested as the first step in infectivity with two mechanisms proposed, one CME (Inoue et al., 2020) with a second study indicating a clathrin-independent process for SARS-CoV entry (Wang et al., 2020). Here we us purified spike protein and lentivirus pseudotyped with SARS-CoV-S glycoprotein to measure endocytosis in HEK-293 cells expressing ACE2 and cells lines with endogenous ACE2 expression. We demonstrate that drugs, which are known inhibitors of CME, block S protein endocytosis and we further demonstrate that knockdown of CHC blocks both S protein endocytosis and pseudovirus infectibility. We thus propose a viral infectivity model involving 3 key steps: 1) the virus uses its S glycoprotein to bind to the plasma membrane of cells expressing ACE2. Notably, a recent paper questions that ACE2 is the cellular receptor for SARS-CoV-2 based on the observation that immunohistochemical analysis

fails to detect ACE2 in cells and tissues that are infectible with virus (Hikmet et al., 2020). Our data does not support this observation.; 2) the ACE2/virus complex undergoes rapid endocytosis with delivery to the lumen of the endosome; 3) fusion of the viral membrane with the lumen of the endosomal membrane allows viral RNA to enter the cytosol for infection. Following entry, the viral particles appear in a pathway that is unique from Trf. Since Trf defines a recycling pathway, we propose the viral capsid protein gets targeted to lysosomes for degradation.

The discovery that CME is an early step in viral infectivity will allow for a new emphasis for drug targets. Chloroquine (CQ) and hydroxychloroquine (HCQ) are widely used malaria drugs that have yielded mixed results for the treatment of COVID-19 (Gao et al., 2020). CQ is known for its efficacy in blocking the CME of nanoparticles (Hu et al., 2020). CQ reduces the expression of the phosphatidylinositol binding CHC assembly protein (PICALM) (Hu et al, 2020) and depletion of PICALM is known to block CME (Miller et al., 2015). HCQ and CQ are in the class of aminoquinolines, which are hemozoin inhibitors, and were identified with other FDA-approved hemozoin inhibitors, including amodiaquine dihydrochloride dihydrate, amodiaquine hydrochloride and mefloquine, in a screen testing for reduction of SARS-CoV-2 infectivity (Weston et al., 2020). Chlorpromazine, which is widely used to treat psychiatric disorders, blocks cellular entry of SARS-CoV and is known to disrupt CME (Inoue et al., 2007). This may explain why psychiatric patients treated with chlorpromazine have a lower incidence of COVID-19 (Plaze et al., 2020). Thus, CME should be considered as a key cellular pathway in any future drug target screens

Materials and Methods

Cell lines

HEK-293T and A549 cell lines were obtained from ATCC (CRL-1573, CCL-185). Adherent Vero-SF-ACF cell line is from ATCC (CCL-81.5) (Kiesslich et. al., 2020). HEK-293T-ACE2 stable cell line was obtained from Dr. Jesse D. Bloom (Crawford et. al., 2020).

Cell culture

All cells were cultured in DMEM high-glucose (GE Healthcare cat# SH30081.01) containing 10% bovine calf serum (GE Healthcare cat# SH30072.03), 2 mM L-glutamate (Wisent cat# 609065, 100 IU penicillin and 100 µg/ml streptomycin (Wisent cat# 450201). Cell lines were monthly checked for mycoplasma contamination using the mycoplasma detection kit (biotool cat# B39038).

Immunoblot

Cells were collected in HEPES lysis buffer (20 mM HEPES, 150 mM sodium chloride, 1% Triton X-100, pH 7.4) supplemented with protease inhibitors. Cells in lysis buffer were gently rocked for 30 minutes (4ºC). Lysates were spun at 238,700xg for 15 min at 4°C and equal protein aliquots of the supernatants were analyzed by SDS-PAGE and immunoblot. Lysates were run om large 5–16% gradient polyacrylamide gels and transferred to nitrocellulose membranes. Proteins on the blots were visualized by Ponceau staining. Blots were then blocked with 5% milk, and antibodies were incubated O/N at 4°C with 5% bovine serum albumin in TBS with 0.1% Tween 20 (TBST). The peroxidase conjugated secondary antibody was incubated in a 1:5000 dilution in TBST with 5% milk for 1 hr at room temperature followed by washes.

Antibodies

SARS-Cov-2 S protein antibody is from GeneTex (GTX632604). ACE2 antibody is from GeneTex (GTX01160). 6x-His Tag antibody is from ThermoFisher Scientific (MA1-21315-D550). GAPDH antibody is from OriGene (TA802519). HSC70 antibody is from Enzo (ADI-SPA-815-F). CHC antibody is from Cell Signaling (4796S). Conjugated Transferrin antibody is from ThermoFisher Scientific (T23366). Alexa Fluor 488, 568 and 647 conjugated secondary antibodies are from Invitrogen.

Confocal microscopy

Cells were grown on poly-L-lysine coated coverslips. Cells were fixed in 4% PFA for 10 min and then washed 3 times with PBS. Cells were then permeabilized in 0.2% Triton X-100 in PBS and blocked with 2% BSA in PBS for 1 hour. Further, coverslips were incubated in a wet chamber with diluted antibody in blocking buffer overnight at 4°C. The following day, cells were washed 3 times and incubated with corresponding Alexa Fluorophore diluted in blocking buffer for 1 h at room temperature. Cells were again washed 3 times with blocking buffer and once with PBS. Nuclei were stained using DAPI (1 µg/ml diluted in blocking buffer) for 10 min. Finally, coverslips were mounted on a slide using mounting media (DAKO, Cat# S3023). Imaging was performed using a Leica TCS SP8 confocal microscope, Zeiss LSM-880 and Opera Phoenix High-Content Screening microscope.

Endocytosis assay using purified spike protein

Cells were incubated at 37°C with serum free starvation media (DMEM) for 3 h to enhance ACE2 receptor expression. Prior to the addition of S protein, cells were cooled to 4°C by being placed on ice. S protein was added to each well (3 ug per 200 ul of media) and incubated on ice for 30 min (to allow ligand attachment to the cell surface). Subsequently, cells were incubated at 37°C (to allow internalization) for indicated time points (transferrin was also added in some experiments in the same manner). Prior to fixation, cells were acid washed (washing off extracellular S protein) or PBS washed for 1 min and rinsed with acid or PBS. Cells were then washed 3 times with PBS followed by fixation for 10 min at 4°C.

siRNA mediated knockdown of CHC

HEK-293T-ACE2 cells (60% confluency) were transfected with siRNA targeted against CHC (Dharmacon; SMARTpool: ON-TARGETplus; L-004001-01-0010) or control siRNA (Dharmacon; ON-TARGETplus CONTROL) using Lipofectamine RNAiMax reagent (Invitrogen, 13778-075). On day 3, cells were processed for immunoblot to investigate the effect of siRNA and parallelly, cells were infected with pseudovirus or used for spike endocytosis assays.

Purified SARS-Cov-2 spike and pseudovirus production

Purified SARS-CoV-2 S protein prefusion-stabilized ectodomain (C-term His tag, with furin cleavage site removed, trimerization stabilized) was produced by LakePharma (#46328). And, lentivirus pseudotyped with SARS-CoV-2 Spike Protein was supplied by VectorBuilder (catalog number: LVL-SARS-CoV-2_S(VB191025-5545hpr)).

Treatments with chemical inhibitors

Cells were washed five times with serum free starvation media (DMEM) to remove any traces of serum. Further, cells were incubated with Dynasore (80 μM; abcam, Ab120192) or Pitstop 2 (15 μM; abcam, ab120687) in serum free media for 30 or 20 min, respectively. DMSO was used as a control for Dynasore and Pitstop 2 negative control (abcam, ab120688). Following incubation, drug containing media was replaced with S protein (3 ug per 200 ul of media) and further incubated for 5 min to allow internalization. Finally, cells were processed for immunofluorescence labeling.

Pseudovirus SARS-Cov-2 infection

293T-ACE2 cells were transfected with control siRNA or siRNA targeted against CHC (Dharmacon) using jetPRIME. Cells were split on day 2 and 10,000 cells were seeded in each well (96 well-plate; CellCarrier-96 Ultra Microplates, Perkinelmer). At 12-14 h after cell seeding, cells were incubated with concentrated pseudovirus SARS-Cov-2 for 12 h. Following this incubation, pseudovirus containing media was replaced with regular DMEM media and incubated further for 48 h. Cells were fixed with 4% PFA for 10 min and stained with DAPI.

Quantification

Internalization of purified spike: Image J was used to measure the fluorescence intensity. The DAPI channel was used to count the number of cells per image. This was done by calculating the maxima using the “Find Maxima” function. The threshold was set at 150. This automated the way in which to count the cells. Then, the spike protein fluorescence corresponding to the cell count was calculated using the “measure” function. Fluorescence was then divided by cell count to calculate the fluorescence per cell in each condition. Infection of cells using pseudovirus SARS-Cov-2: GFP expressing cells in CellCarrier-96 Ultra Microplate were imaged using Opera Phoenix HCS (40x objective). Each well was split into 310 grids and imaged. The total number of GFP expressing cells in each condition was normalized to the total number of cells in the respective wells.

Statistics

Graphs were prepared using GraphPad Prism 6 software. For all data, comparisons were made using student’s T-test. All data are shown as the mean +/- SEM with $P < 0.05$ considered statistically significant.

Acknowledgments

We acknowledge the Neuro Microscopy Imaging Centre and Advanced BioImaging Facility at McGill University. We thank Dr. Jesse D. Bloom (University of Washington, Seattle) for HEK-293T-ACE2 stable cell line and Dr. Amine A. Kamen (Department of Bioengineering, McGill University) for Vero ATCC CCL 81.5 cell line. This work was supported by a grant from the Natural Sciences and Engineering Research Council to PSM. AB is supported by a studentship from the Parkinson's Society of Canada. RK is supported by a studentship from ALS Canada. VF was supported by a fellowship from the Fonds de recherche Sante. PSM is a James McGill Professor and a Fellow of the Royal Society of Canada.

References

Bendavid, E., Mulaney, B., Sood, N., Shah, S., Ling, E., Bromley-Dulfano, R., Lai, C., Weissberg, Z., Saavedra-Walker, R., Tedrow, J., Tversky, D., Bogan, A., Kupiec, T., Eichner, D., Gupta, R., Ioannidis, J. and Bhattacharya, J. (2020) COVID-19 Antibody Seroprevalence in Santa Clara County, California. *medRxiv* **doi**: https://doi.org/10.1101/2020.04.14.20062463.

Goodman, J.D. and Rothfeld, M. (2020) 1 in 5 New Yorkers May Have Had Covid-19, Antibody Tests Suggest**.** New York Times, April 24, Section A, Page 1.

Zaki, A.M., van Boheemen, S., Bestebroer, T.M., Osterhaus, A.D. and Fouchier, R.A.(2012) Isolation of a novel coronavirus from a man with pneumonia in Saudi Arabia. *N. Engl. J. Med*. **367**:1814-1820.

Drosten, C., Günther, S., Preiser, W., van der Werf, S., Brodt, H.R., Becker, S., Rabenau, H., Panning, M., Kolesnikova, L., Fouchier, R.A., Berger, A., Burguière, A.M., Cinatl, J., Eickmann, M., Escriou, N., Grywna, K., Kramme, S., Manuguerra, J.C., Müller, S., Rickerts, V., Stürmer, M., Vieth, S., Klenk, H.D., Osterhaus, A.D., Schmitz, H. and Doerr, H.W. (2003) Identification of a novel coronavirus in patients with severe acute respiratory syndrome. *N. Engl. J. Med.* **348**:1967-1976.

Ksiazek, T.G., Erdman, D., Goldsmith, C.S., Zaki, S.R., Peret, T., Emery, S., Tong, S., Urbani, C., Comer, J.A., Lim, W., Rollin, P.E., Dowell, S.F., Ling, A.E., Humphrey, C.D., Shieh, W.J., Guarner, J., Paddock, C.D., Rota, P., Fields, B., DeRisi, J., Yang, J.Y., Cox, N., Hughes, J.M., LeDuc, J.W., Bellini, W.J. and Anderson, L.J.; SARS Working Group. (2003) A novel coronavirus associated with severe acute respiratory syndrome. *N. Engl. J. Med.* **348**:1953-1966.

Huang, C., Wang, Y., Li, X., Ren, L., Zhao, J., Hu, Y., Zhang, L., Fan, G., Xu, J., and Gu, X. (2020). Clinical features of patients infected with 2019 novel coronavirus in Wuhan, China. *Lancet* **395**:497-506.

Zhu, N., Zhang, D., Wang, W., Li, X., Yang, B., Song, J., Zhao, X., Huang, B., Shi, W., and Lu, R. (2020) A Novel coronavirus from patients with pneumonia in China. *N. Engl. J. Med*. **382**:727–733.

Tortorici, M.A. and Veesler, D. (2019). Structural insights into coronavirus entry. *Adv. Virus Res.* **105**:93-116.

Sun H, Xiao Y, Liu J, Wang D, Li F, Wang C, Li C, Zhu J, Song J, Sun H, Jiang Z, Liu L, Zhang X, Wei K, Hou D, Pu J, Sun Y, Tong Q, Bi Y, Chang KC, Liu S, Gao GF, Liu J. (2020) Prevalent Eurasian avian-like H1N1 swine influenza virus with 2009 pandemic viral genes facilitating human infection. *Proc. Natl. Acad. Sci. USA* **doi**:10.1073/pnas.1921186117.

Wrapp, D., Wang, N., Corbett, K.S., Goldsmith, J.A., Hsieh, C.L., Abiona, O., Graham, B.S. and McLellan, J.S. (2020) Cryo-EM structure of the 2019-nCoV spike in the prefusion conformation. *Science* **367**:1260-1263.

Hoffmann, M., Kleine-Weber, H., Schroeder, S., Krüger, N., Herrler, T., Erichsen, S., Schiergens, T.S., Herrler, G., Wu, N.H., Nitsche, A., Müller, M.A., Drosten, C. and Pöhlmann, S (2020) SARS-CoV-2 cell entry depends on ACE2 and TMPRSS2 and is blocked by a clinically proven protease inhibitor. *Cell* **181**:271-280.

Letko, M., Marzi, A. and Munster, V. (2020) Functional assessment of cell entry and receptor usage for SARS-CoV-2 and other lineage B betacoronaviruses. *Nat. Microbiol*. **5**:562-569.

Zhou, P., Yang, X.L., Wang, X.G., Hu, B., Zhang, L., Zhang, W., Si, H.R., Zhu, Y., Li, B., Huang, C.L., Chen, H.D., Chen, J., Luo, Y., Guo, H., Jiang, R.D., Liu, M.Q., Chen, Y., Shen, X.R., Wang, X., Zheng, X.S., Zhao, K., Chen, Q.J., Deng, F., Liu, L.L., Yan, B., Zhan, F.X., Wang, Y.Y., Xiao, G.F. and Shi, Z.L. (2020) A pneumonia outbreak associated with a new coronavirus of probable bat origin. *Nature* **579**:270-273.

Walls, A.C., Xiong, X., Park, Y.J., Tortorici, M.A., Snijder, J., Quispe, J., Cameroni, E., Gopal, R., Dai, M., Lanzavecchia, A., Zambon, M., Rey, F.A., Corti, D. and Veesler, D. (2019) Unexpected receptor functional mimicry elucidates activation of coronavirus fusion. *Cell* **176**:1026-1039.

Hamming, I., Timens, W., Bulthuis, M.L., Lely, A.T., Navis, G. and van Goor, H. (2004) *J. Pathol.* **203**:631-637.

Weber, T., Zemelman, B.V., McNew, J.A., Westermann, B., Gmachl, M., Parlati, F., Söllner, T.H. and Rothman, J.E. (1998) SNAREpins: minimal machinery for membrane fusion. *Cell* **92**:759-772.

Tang, T., Bidon, M., Jaimes, J.A., Whittaker, G.R., and Daniel, S. (2020) Coronavirus membrane fusion mechanism offers a potential target for antiviral development. *Antiviral Res*. **doi**:10.1016/j.antiviral.2020.104792

Glebov, O. (2020) Understanding SARS-CoV-2 endocytosis for COVID-19 drug repurposing. *The FEBS J*. **doi**.org/10.1111/febs/15369

Yang, N. and Shen, H.-M. (2020) Targeting the endocytic pathway and autophagy process as a novel therapeutic strategy in COVID-19. *Int. J. Biol. Sci.* **16**:1724–1731.

Inoue, Y., Tanaka, N., Tanaka, Y., Inoue, S., Morita, K., Zhuang, M., Hattori, T. and Sugamara, T. (2007) Clathrin-Dependent Entry of Severe Acute Respiratory Syndrome Coronavirus into Target Cells Expressing ACE2 with the Cytoplasmic Tail Deleted. *J. Virol.* **81:**8722–8729.

Wang, H., Yang, P., Liu, K., Guo, Z., Zhang, Y., Zhang, G. and Jiang, C. (2008) SARS coronavirus entry into host cells through a novel clathrin- and caveolae-independent endocytic pathway. *Cell Research* **18**: 290–301.

Crawford, H.D.K., Eguia, R., Dingens, A.S., Loes, A.N., Malone, K.D., Wolf, C.R., Chu, H.Y., Tortorici, M.A., Veesler, D., Murphy, M., Pettie, D., King, N.P., Balazs, A.B. and Bloom, J.D. (2020) Protocol and reagents for pseudotyping lentiviral particles with SARS-CoV-2 Spike protein for neutralization assays. *BioXriv* **doi**.org/10.1101/2020.04.20.051219.

Li, H-S., Stolz, D.B. and Romero, G. (2005) Characterization of endocytic vesicles using magnetic microbeads coated with signaling ligands. *Traffic* **6**:324-334.

Marcia, E., Ehrlich, M., Massol, R., Boucrot, E., Brunner, C. and Kirchhausen, T. (2006) Dynasore, a cell-permeable inhibitor of dynamin. *Dev. Cell* **10**:839-850.

von Kleist, L., Stahlschmidt, W., Bulut, H., Gromova, K., Puchkov, D., Robertson, M.J., MacGregor, K.A., Tomilin, N., Pechstein, A., Chau, N., Chircop, M., Sakoff, J., von Kries, J.P., Saenger, W., Kräusslich, H.G., Shupliakov, O., Robinson, P.J., McCluskey, A. and Haucke, V. (2011) Role of the clathrin terminal domain in regulating coated pit dynamics revealed by small molecule inhibition. *Cell* **146**:471-484.

Park, R.J., Shen, H., Liu, L., Liu, X., Ferguson, S.M. and De Camilli, P. (2013) Dynamin triple knockout cells reveal off target effects of commonly used dynamin inhibitors. *J. Cell Sci*. **126**:5305-5312

Lemmon, S.K. and Traub, L.M. (2012) Getting in touch with the clathrin terminal domain. *Traffic* **13**:511-519.

Galvez, T., Teruel, M.N., Do Heo, W., Jones, J.T., Kim, M., Liou, J., Myers J.W. and Meyer, T. (2007) siRNA screen of the human signaling proteome identifies the PtdIns(3,4,5)P3-mTOR signaling pathway as a primary regulator of transferrin uptake. *Genome Biology* **doi**:10.1186/gb-2007-8-7-r142.

Kim, M.L., Sorg, I. and Arrieumerlou, C. (2011) Endocytosis-independent function of clathrin heavy chain in the control of basal NF-kB activation. *PLoS ONE*. **doi**:10.1371/journal.pone.0017158

Stoorvogel, W., Strous, G.J., Ciechanover, A. and Schwartz, A.L. (1991) Trafficking of the transferrin receptor. *Targeted Diagn. Ther*. **4**:267-304.

Kang, Y-L., Chou, Y-Y., Rothlauf, P.W., Liu, Z., Piccinotti, Z., Soh, T.K., Cureton, D., Case, J.B., Chen, R.E., Diamond, M.S., Whelan, S.P.J. and Kirchhausen, T. (2020). Inhibition of PIKfyve kinase prevents infection 1 by EBOV and SARS2 CoV-2. *bioXriv* **doi**.org/10.1101/2020.

Pelkmans, L. and Helenius, A. (20030 Insider information: what viruses tell us about endocytosis. *Curr. Opin. Cell Biol*. **15**:414–422.

Yamauchi, Y. and Helenius, A. (2013) . Virus entry at a glance. *J. Cell Sci*. **126**:1289-1295.

Marsh, M. and Helenius, A. (2006) Virus Entry: Open Sesame. *Cell* **124**:729–740.

Hikmet, F., Méar, L., Uhlén, M. and Lindskog, C. (2020). The protein expression profile of ACE2 in human tissues. *BioXriv* **doi**.org/10.1101/2020.03.31.016048doi:

Gao, J., Tian, Z., and Yang, X. (2020) Breakthrough: Chloroquine phosphate has shown apparent efficacy in treatment of COVID-19 associated pneumonia in clinical studies. *BioSci. Trends*. **16**:73-73.

Hu, T.Y., Frieman, M., and Wolfram, J. (2020) Insights from nanomedicine into chloriquine efficacy against COVID-19. *Nat. Nanotech*. **doi**.org/10.1038/s41565-020-0674-9.

Miller, S.E., Mathiasen, S., Bright, N.A., Pierre, F., Kelly, B.T., Kladt, N., Schauss, A., Merrifield, C.J., Stamou, D., Höning, S. and Owen, D.J. (2015) CALM regulates clathrin-coated vesicle size and maturation by directly sensing and driving membrane curvature. *Dev. Cell* 33:163–175.
Weston, S., Coleman, C.M., Haupt, R., Logue, J., Matthews, K. and Frieman, M.B. (2020) Broad anti-coronaviral activity of FDA approved drugs against SARS-CoV-2 in vitro and SARS-CoV in vivo. *BioRxiv* **doi**.org/10.1101/2020.

Plaze, M., Attali, D., Petita, A-C., Blatzerd, M., Simon-Lorieree, E., Vinckiera, F., Cachia, A., Chrétiend, F. and Gaillard, R. (2020) Repositionnement de la chlorpromazine dans le traitement du COVID-19 : étude reCoVery. *L'Encéphale* (In press).

Kiesslich, S., Losa, J.P. V-C., Gelinas, J-F. and Kamen, A.A. (2020) Serum-free production of rVSV-ZEBOV in Vero cells: Microcarrier bioreactor versus scale-X hydron fixed bed. *J. Biotech*. **310**:32-29.

Figure legends

Figure 1. SARS-CoV-2 spike protein binds to the surface of HEK-293 cells expressing ACE2. (A) HEK-293 cells, wild-type (top row of images) or stably expressing ACE2 (bottom row of images) were incubated with purified, His6-tagged spike protein and with alexa-647 labelled transferrin for 30 min at 4°C. Following PBS wash, the cells were fixed and stained with DAPI to reveal nuclei, with an antibody selectively recognizing ACE2, and with an antibody recognizing the His6 epitope tag of the spike protein. Scale bars = 40 μm for the low mag images and 10 μm for the higher mag inset of the composite. **(B)** Experiment performed as in **A** except that the HEK-293 cells were briefly acid washed prior to fixation. Scale bars = 40 μm for the low mag images and 10 μm for the higher mag inset of the composite.

Figure 2. SARS-CoV-2 spike protein enters cells in an ACE2-dependent manner. HEK-293 cells, wild-type (top row of images) or stably expressing ACE2 (bottom row of images) were incubated with purified, His6-tagged spike protein and with alexa-647 labelled transferrin for 30 min at 4°C. The cells were then transferred to 37°C for 30 min. The cells were returned to ice and following PBS wash, were fixed and stained with DAPI to reveal nuclei, with an antibody selectively recognizing ACE2, and with an antibody recognizing the His6 epitope tag of the spike protein. Scale bars = 40 μm for the low mag images and 10 μm for the higher mag inset of the composite.

Figure 3. Time course of SARS-CoV-2 spike protein entry into cells. HEK-293 cells stably expressing ACE2 were incubated with purified, His6-tagged spike protein for 30 min at 4°C. The cells were then transferred to 37°C for the indicated time periods before being returned to ice. Following PBS wash, cells were fixed and stained with DAPI to reveal nuclei and with antibody selectively recognizing the His6 epitope tag of the spike protein. Scale bars = 40 μm for the low mag images and 10 μm for the higher mag insets on the right.

Figure 4. SARS-CoV-2 spike protein endocytosis is blocked by chemical inhibitors of CME. (A) HEK-293 cells stably expressing ACE2 were incubated with purified, His6-tagged spike protein for 30 min at 4°C. The cells were then transferred to 37°C for 30 min before being returned to ice. Following PBS wash, cells were fixed and stained with DAPI to reveal nuclei and with antibody selectively recognizing the His6 epitope tag of the spike protein. Inhibitors of

clathrin-mediated endocytosis or their controls, as indicated, were added to the cells 30 min prior to the addition of spike protein. Scale bars = 40 μm for the low mag images and 10 μm for the higher mag insets on the right. **(B)** Quantification of experiments performed as in **A**. n=15 for Dynasore and n=14 for Pitstop 2 from three independent experiments, mean ± SEM; unpaired t-test; ****, $p < 0.0001$.

Figure 5. SARS-CoV-2 spike protein endocytosis is blocked by CHC knockdown. (A) HEK-293 cells stably expressing ACE2 were transfected with control siRNA or with an siRNA established to selectively knockdown the expression of CHC. Cell lysates were prepared and blotted with the indicated antibodies. **(B)** HEK-293 cells stably expressing ACE2, transfected with a control siRNA or an siRNA driving CHC knockdown, were incubated with purified, His6-tagged spike protein for 30 min at 4°C. The cells were then transferred to 37°C for 30 min before being returned to ice. Following PBS wash, cells were fixed and stained with DAPI to reveal nuclei and with antibodies selectively recognizing CHC and the His6 epitope tag of the spike protein. Scale bars = 40 μm for the low mag images and 10 μm for the higher mag insets on the right. **(C)** Quantification of experiments performed as in **B**. n=7 from three independent experiments, mean ± SEM; unpaired t-test; ***, $p < 0.001$.

Figure 6. SARS-CoV-2 spike protein is rapidly endocytosed in VERO cells. (A) Lysates were made from HEK-293T cells, wild-type or expressing ACE2, VERO cells and A549 cells, and were immunoblotted with an antibody specifically recognizing ACE2. **(B)** VERO cells were incubated with purified, His6-tagged spike protein for 30 min at 4°C. The cells were then transferred to 37°C for the indicated time periods before being returned to ice. Following acid wash, cells were fixed and stained with DAPI to reveal nuclei and with antibody selectively recognizing spike protein. Scale bars = 40 μm for the low mag images and 10 μm for the higher mag insets on the right.

Figure 7. SARS-CoV-2 spike protein is rapidly endocytosed in A549 cells. A549 cells were incubated with purified, His6-tagged spike protein for 30 min at 4°C. The cells were then transferred to 37°C for the indicated time periods before being returned to ice. Following acid wash, cells were fixed and stained with DAPI to reveal nuclei and with antibody selectively recognizing spike protein. Scale bars = 40 μm for the low mag images and 10 μm for the higher mag insets on the right.

Figure 8. SARS-CoV-2 spike protein follows a trafficking itinerary distinct from transferrin. HEK-293 cells stably expressing ACE2 were incubated with purified, His6-tagged spike protein and Trf-Alexa647 for 30 min at 4°C. The cells were then transferred to 37°C for the indicated time periods before being returned to ice. Following PBS wash, cells were fixed and stained with DAPI to reveal nuclei and with antibody selectively recognizing the His6 epitope tag of the spike protein. Scale bars = 40 μm for the low mag images and 10 μm for the higher mag insets on the right.

Figure 9. Lentivirus pseudotyped with SARS-CoV-2 S glycoprotein requires CHC for infectivity. **(A)** Quantification of SARS-Cov-2 pseudovirus infection in 293T-ACE2 and 293T cells from three independent experiments (mean ± SEM; unpaired t-test; ***, $p < 0.001$). **(B)** Graph showing quantification of SARS-Cov-2 pseudovirus infection in control and CHC knockdown 293T-ACE2 cells from three independent experiments (mean ± SEM; unpaired t-test; **, $p < 0.01$).

Supplemental Figure 1. The antibody against SARS-CoV-2 S protein specifically recognizes internalized protein. HEK-293 cells stably expressing ACE2 were incubated with purified, His6-tagged spike protein for 30 min at 4°C. The cells were then transferred to 37°C for the indicated time periods before being returned to ice. Following acid wash, cells were fixed and stained with DAPI to reveal nuclei and with antibody recognizing the His6 epitope tag of the S protein and with antibody directed against the S protein. Scale bars = 40 μm for the low mag images and 10 m for the higher mag insets on the right.

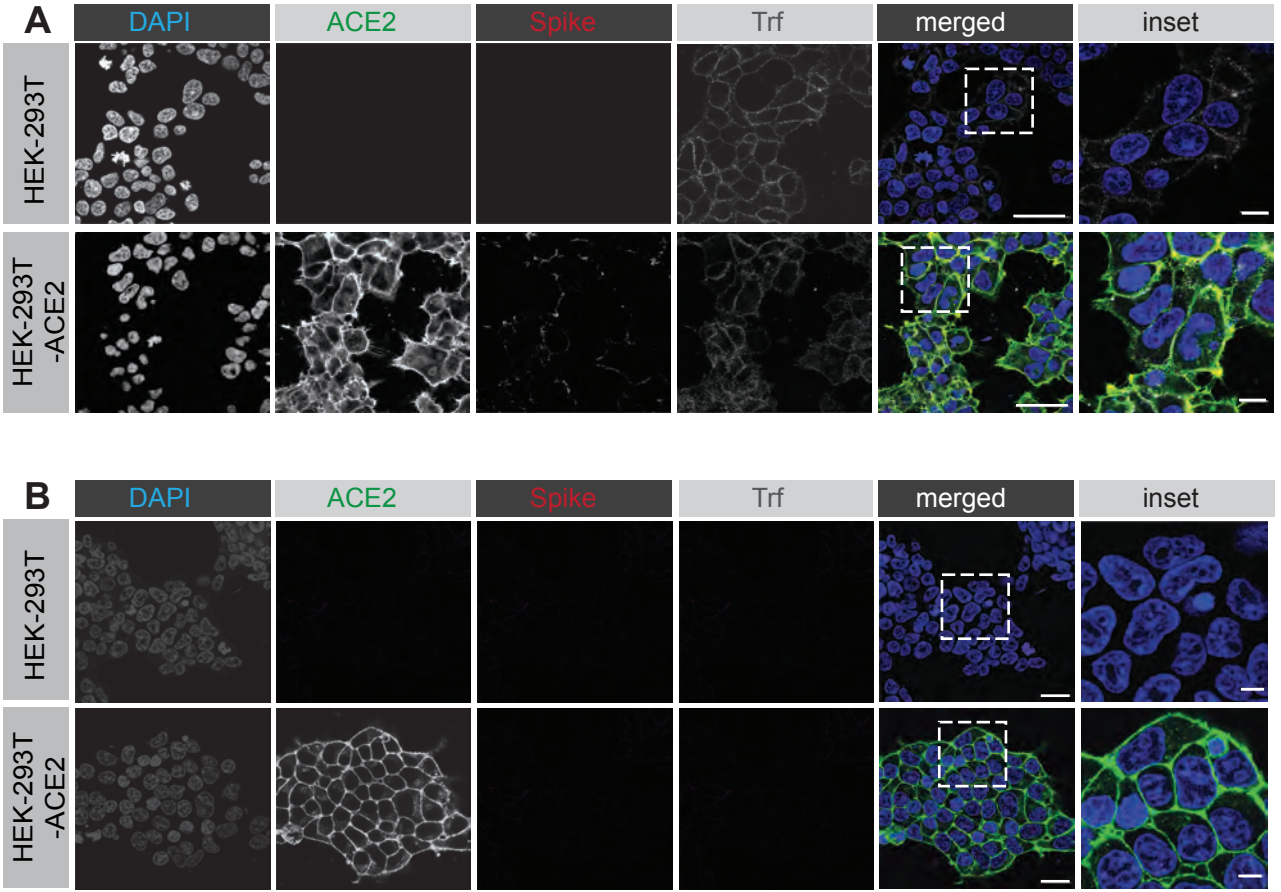

Bayati et. al. Figure 1

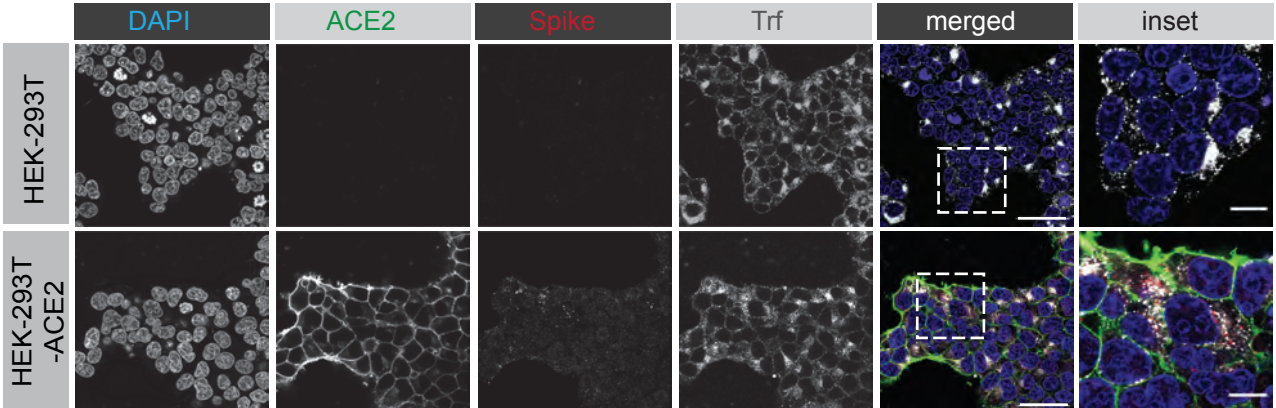

Bayati et. al. Figure 2

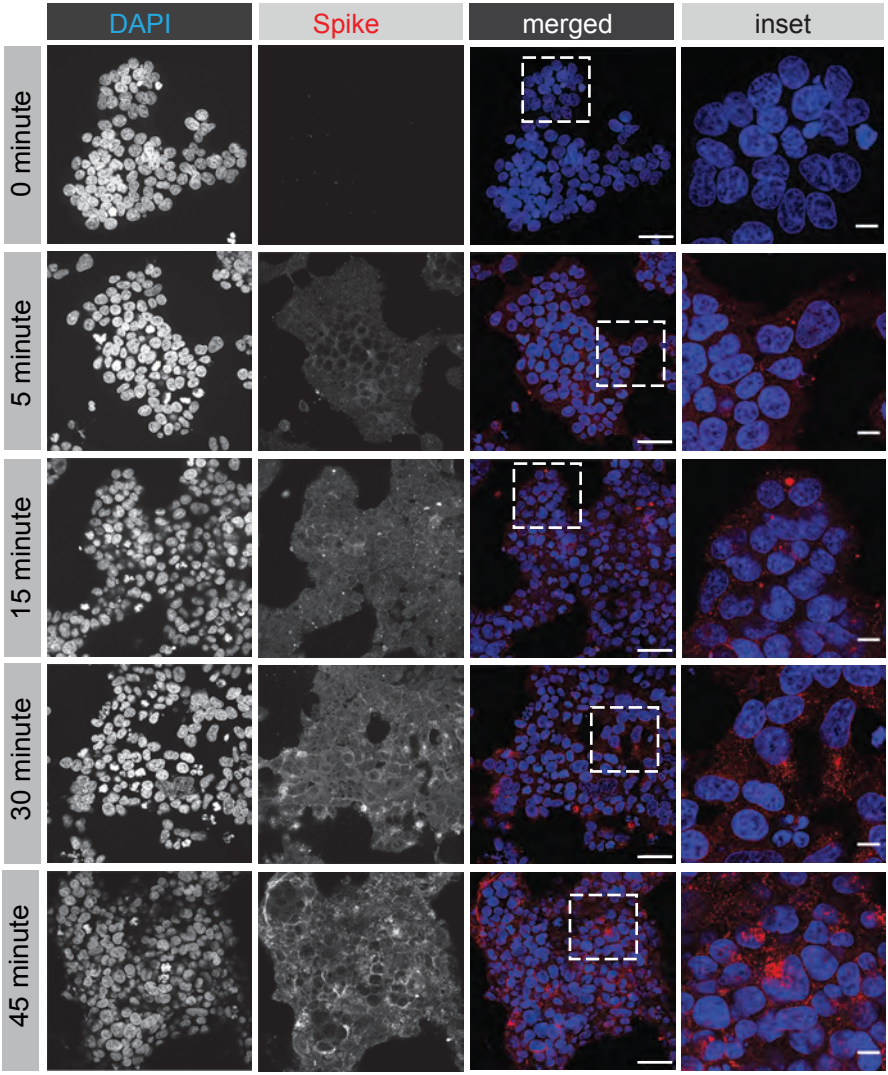

Bayati et. al. Figure 3

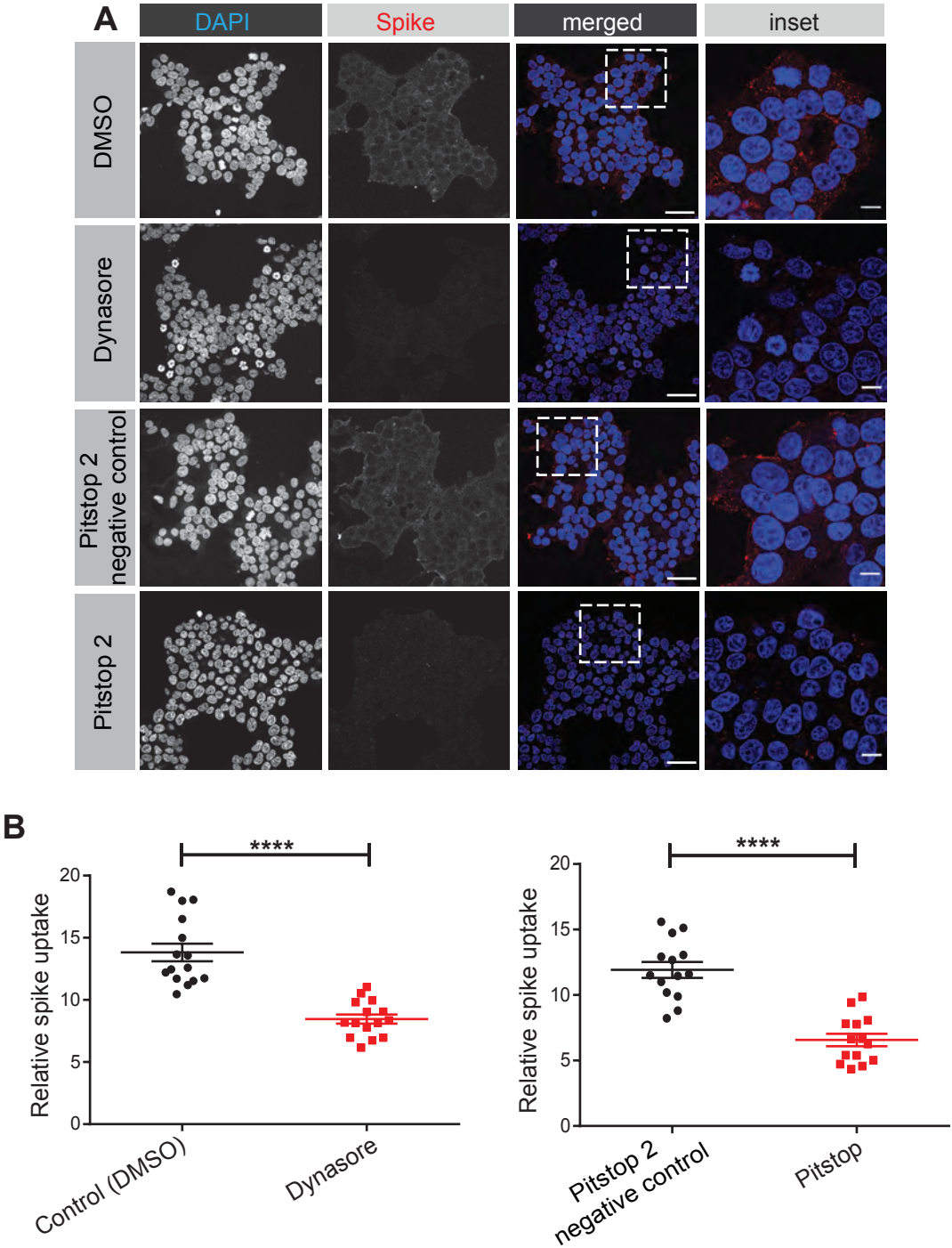

Bayati et. al. Figure 4

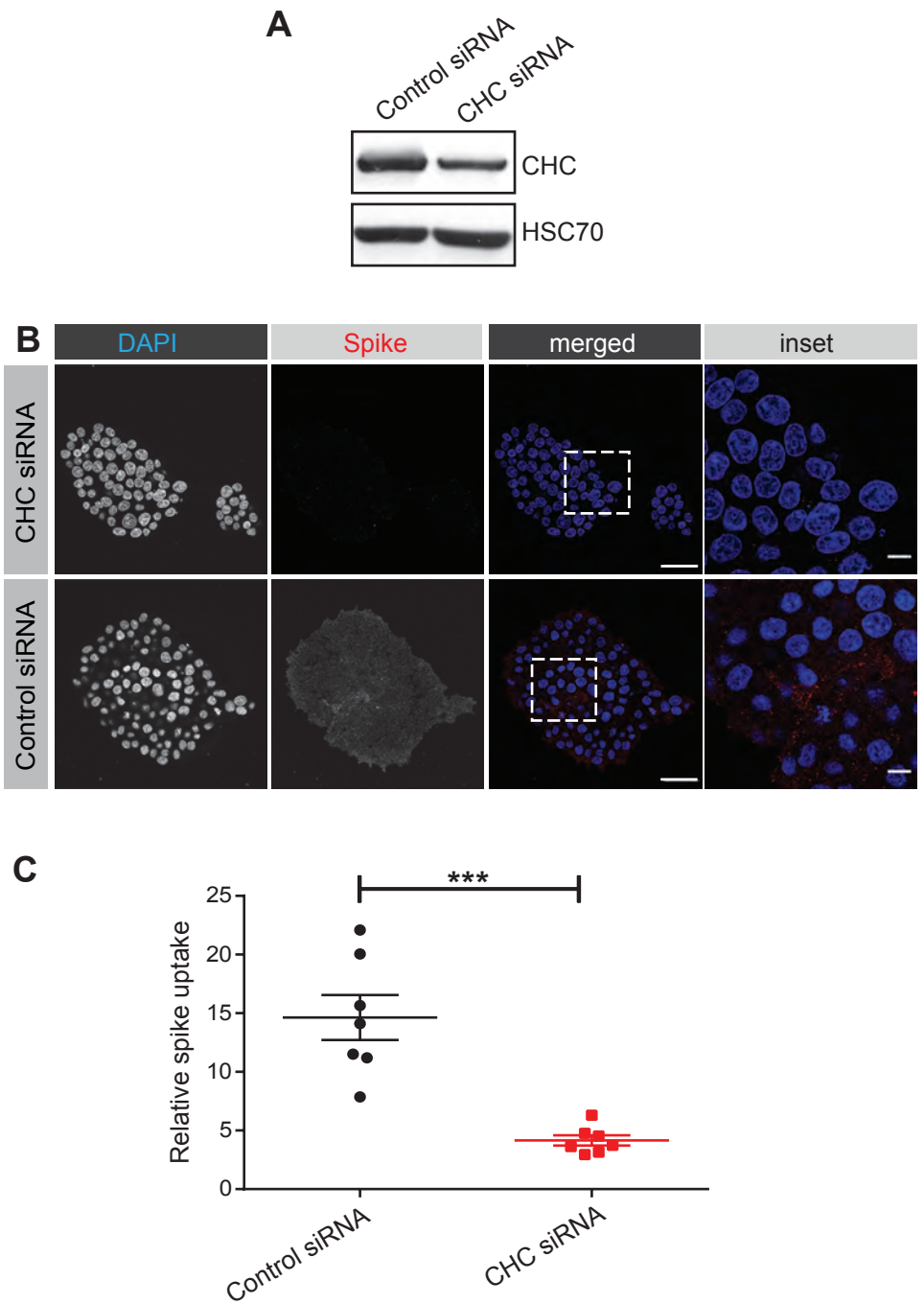

Bayati et. al. Figure 5

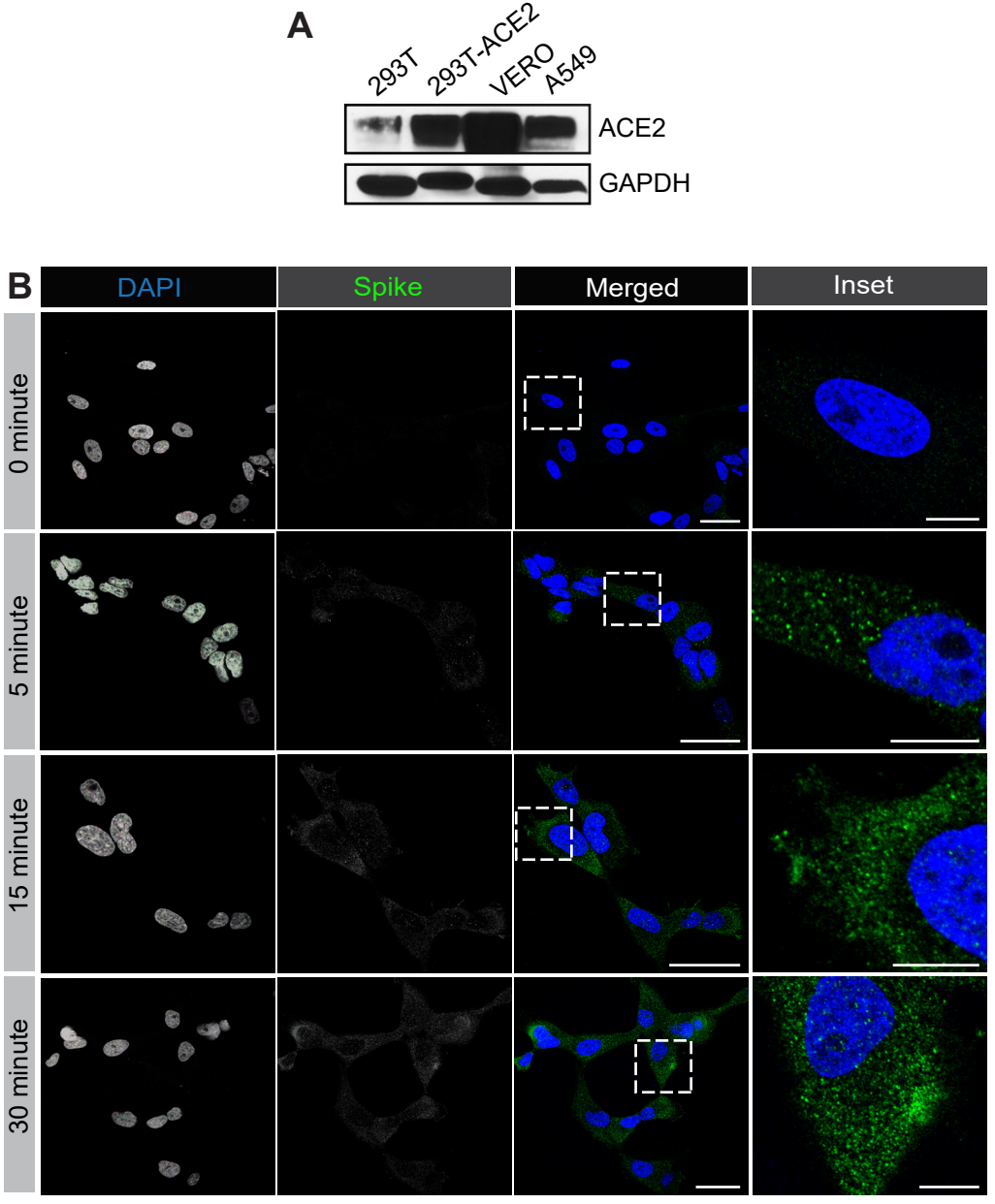

Bayati et al., Figure 6

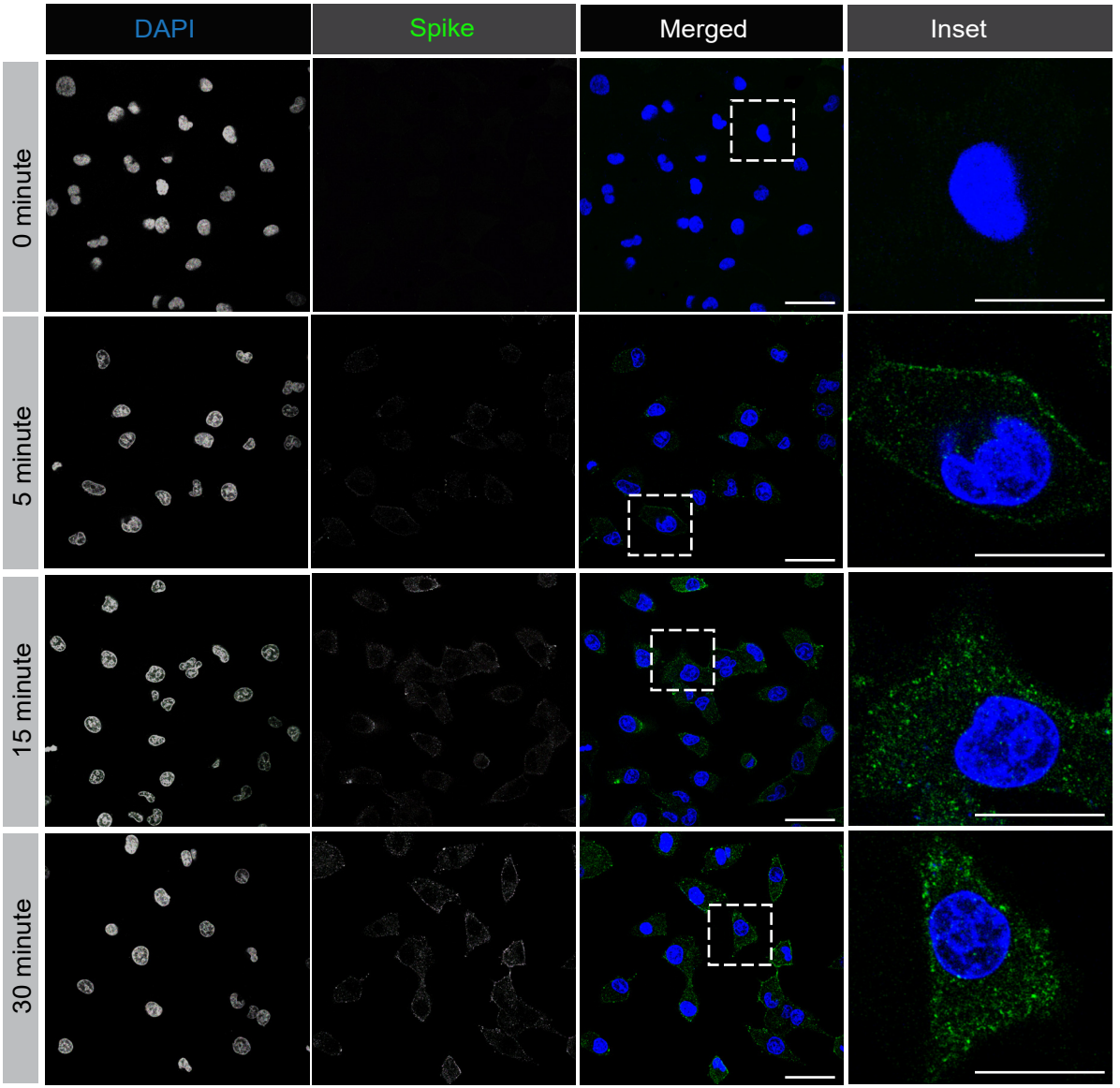

Bayati et al., Figure 7

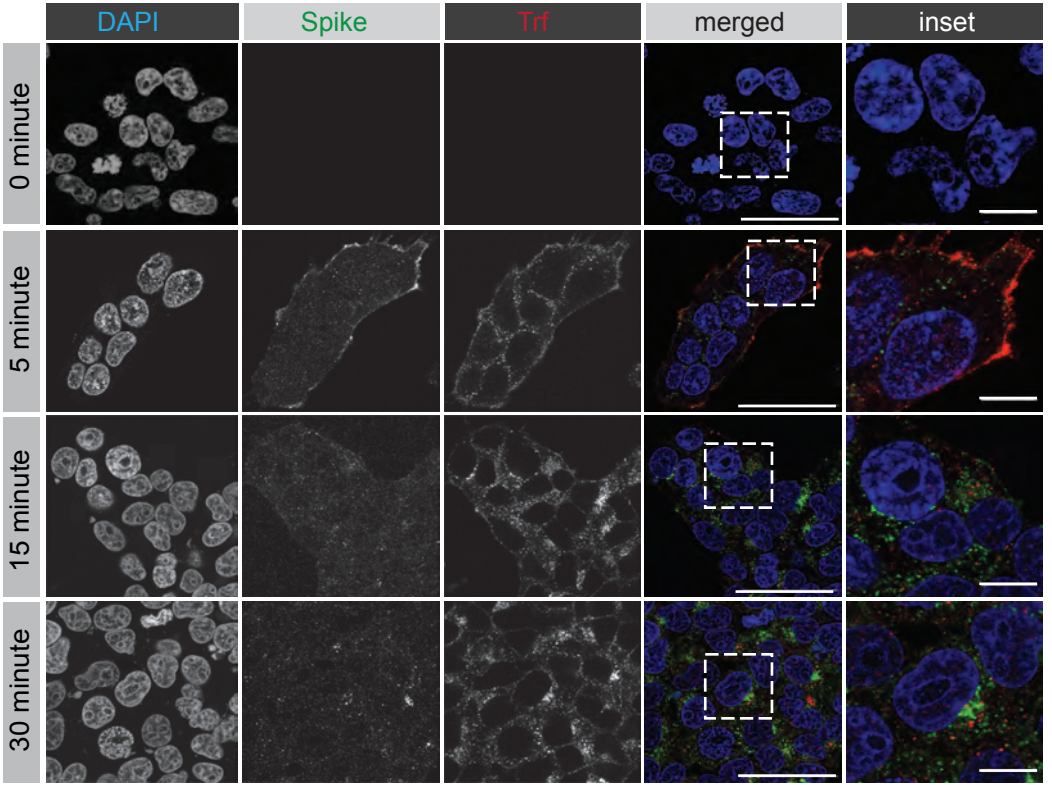

Bayati et. al. Figure 8

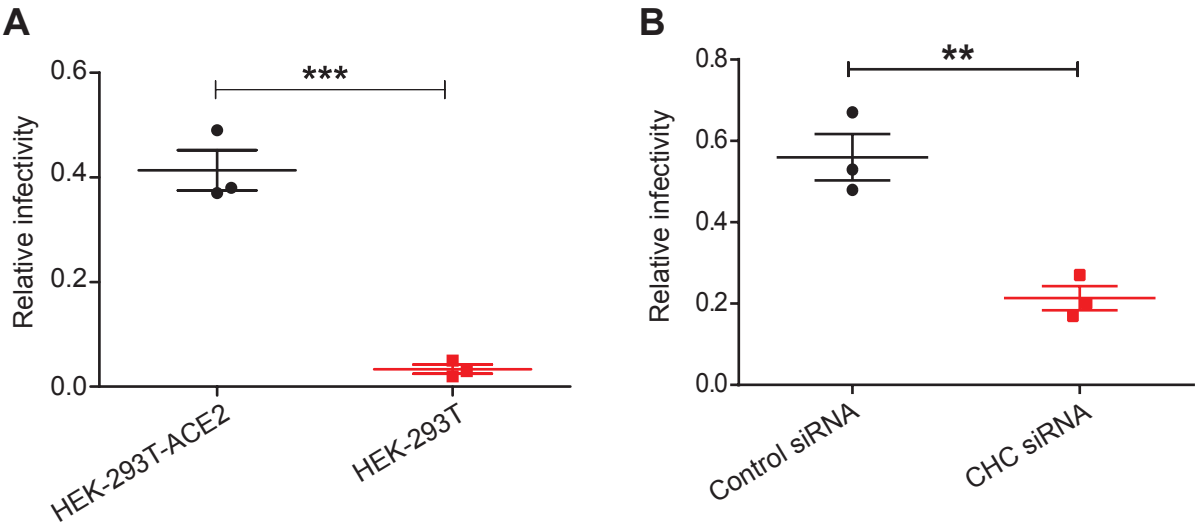

Bayati et. al. Figure 9

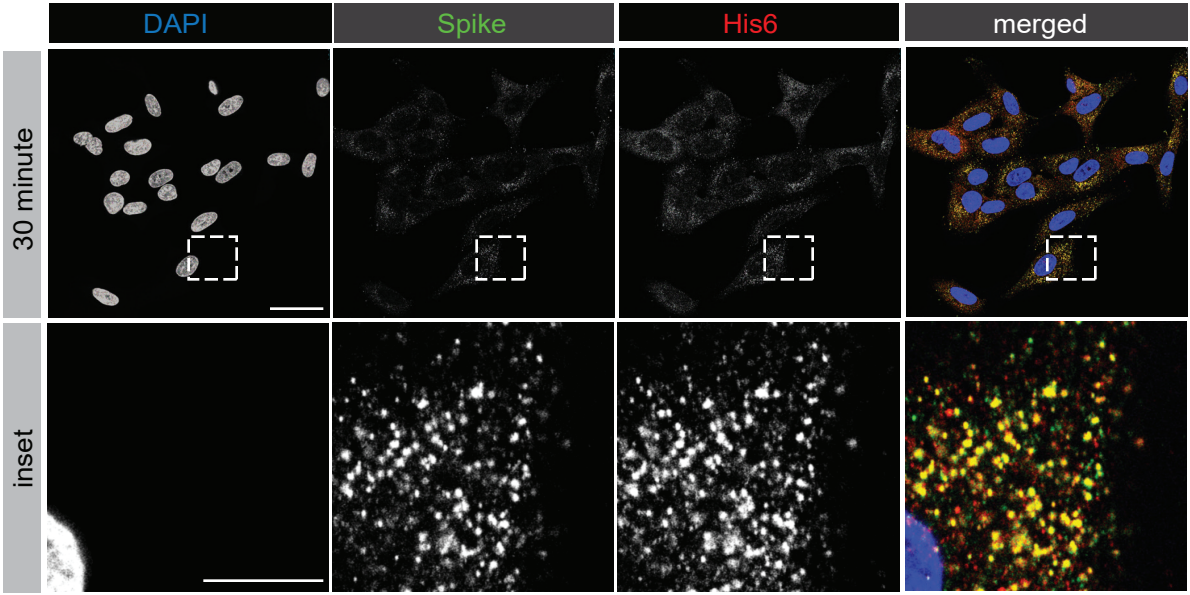

Bayati et al., Supp Fig.1